THE JOURNAL OF BIOLOGICAL CHEMISTRY VOL. 284, NO. 7, pp. 4695–4704, February 13, 2009

Mutation of Histidine 105 in the T1 Domain of the Potassium Channel Kv2.1 Disrupts Heteromerization with Kv6.3 and Kv6.4*[S]

Received for publication, November 19, 2008, and in revised form, December 5, 2008 Published, JBC Papers in Press, December 11, 2008, DOI 10.1074/jbc.M808786200

Michael Mederos y Schnitzler[‡], Susanne Rinné[§], Lennart Skrobek[‡], Vijay Renigunta[§], Günter Schlichthörl[§], Christian Derst[§], Thomas Gudermann[‡], Jürgen Daut[§1], and Regina Preisig-Müller[§]

From the [‡]Institute of Pharmacology and Toxicology and the [§]Institute of Physiology, Marburg University, 35032 Marburg, Germany

The voltage-activated K^+ channel subunit Kv2.1 can form heterotetramers with members of the Kv6 subfamily, generating channels with biophysical properties different from homomeric Kv2.1 channels. The N-terminal tetramerization domain (T1) has been shown previously to play a role in Kv channel assembly, but the mechanisms controlling specific heteromeric assembly are still unclear. In Kv6.x channels the histidine residue of the zinc ion-coordinating C3H1 motif of Kv2.1 is replaced by arginine or valine. Using a yeast two-hybrid assay, we found that substitution of the corresponding histidine 105 in Kv2.1 by valine (H105V) or arginine (H105R) disrupted the interaction of the T1 domain of Kv2.1 with the T1 domains of both Kv6.3 and Kv6.4, whereas interaction of the T1 domain of Kv2.1 with itself was unaffected by this mutation. Using fluorescence resonance energy transfer (FRET), interaction could be detected between the subunits Kv2.1/Kv2.1, Kv2.1/Kv6.3, and Kv2.1/Kv6.4. Reduced FRET signals were obtained after co-expression of $Kv2.1^{H105V}$ or $Kv2.1^{H105R}$ with Kv6.3 or Kv6.4. Wild-type Kv2.1 but not $Kv2.1^{H105V}$ could be co-immunoprecipitated with Kv6.4. Co-expression of dominant-negative mutants of Kv6.3 reduced the current produced Kv2.1, but not of $Kv2.1^{H105R}$ mutants. Co-expression of Kv6.3 or Kv6.4 with wt Kv2.1 but not with $Kv2.1^{H105V}$ or $Kv2.1^{H105R}$ changed the voltage dependence of activation of the channels. Our results suggest that His-105 in the T1 domain of Kv2.1 is required for functional heteromerization with members of the Kv6 subfamily. We conclude from our findings that Kv2.1 and Kv6.x subunits have complementary T1 domains that control selective heteromerization.

Voltage-gated potassium channels of the Kv family are strongly expressed in the mammalian central nervous system, in the immune system, in muscle cells and in many other cell types. The members of the Kv channel family differ in their time courses of activation and inactivation and in their pharmacological properties. They play a key role in controlling neuronal excitability and regulate a variety of electrophysiological properties, such as the interspike membrane potential, the waveform of the action potential and the firing frequency (1). Most neurons express multiple Kv channel subtypes belonging to one or more subfamilies (2–4). Kv channels are composed of four subunits that surround the central ion permeation pathway. Each subunit has six transmembrane domains (S1–S6) and a pore region containing the signature sequence GYG characteristic for potassium channels (5). Post-translational assembly of tetrameric Kv channels takes place in the ER[2] membrane; subsequently the channels traffic to the plasma membrane (6, 7). A highly conserved sequence in the cytoplasmic N terminus of Kv channels, the tetramerization domain or T1 domain, has been shown to play an important role in channel assembly (6, 8). The T1 domain contains some of the molecular determinants for subfamily-specific homo- or heterotetrameric assembly of Kv α-subunits (9–11). The most striking difference between the T1 domains of Kv1 (*Shaker*) and Kv2–4 (*non-Shaker*) channels is the presence of intersubunit-coordinated Zn^{2+} ions at the assembly interface in non-Shaker channels. The Zn^{2+} ions are coordinated by a C3H1 motif embedded in a conserved sequence motif ($HX_5CX_{20}CC$) of the T1 domain, which is located near the distal end of the N terminus (12–14). These four amino acids are exposed on the subunit interface, with one histidine and two cysteine residues belonging to one subunit and one cysteine residue belonging to the neighboring subunit (12). The T1 domain facilitates tetrameric assembly of Kv channels. Kv subunits in which the T1 has been deleted have been reported to assemble in a promiscuous way via their transmembrane domains and to form stable, functional channels, but both the rates and the efficiency of channel assembly are significantly lower in the mutant channels as compared with their wild-type counterparts (7, 15). Heteromeric assembly of channel subunits is a potential source of diversity of K^+ channel properties. The voltage-activated potassium channel subunits

* This study was supported by the Medizinstiftung (to M. M. S. and R. P. M.), P.E.-Kempkes-Stiftung (to R. P. M.), and SFB593 (TP A3, to T. G.; TP A4, to J. D.). The costs of publication of this article were defrayed in part by the payment of page charges. This article must therefore be hereby marked "*advertisement*" in accordance with 18 U.S.C. Section 1734 solely to indicate this fact.

[S] The on-line version of this article (available at http://www.jbc.org) contains supplemental Figs. S1 and S2.

[1] To whom correspondence should be addressed: Institute of Physiology, Marburg University, Deutschhausstr. 2, 35037 Marburg, Germany. Tel.: 49-6421-2866494; E-mail: jdaut@staff.uni-marburg.de.

[2] The abbreviations used are: ER, endoplasmic reticulum; CHO-K1, chinese hamster ovary K1; E(G/C/Y)FP, enhanced (green/cyan/yellow) fluorescence protein; FRET, fluorescence resonance energy transfer; GAPDH, glyceraldehyde-3-phosphate dehydrogenase; HEK293, human embryonic kidney; IRES, internal ribosome entry site; (q/RT-)PCR, (quantitative/reverse transcription-) polymerase chain reaction; rE, relative expression; wt, wild-type; aa, amino acids; Y2H, yeast two-hybrid.

Kv2.1 and Kv2.2 are capable of heteromeric assembly with members of the Kv6 subfamily, which generates channels with different biophysical properties compared with homomeric Kv2.1 channels (16–20). In the present study we used fluorescence energy resonance transfer (FRET), yeast two-hybrid analysis, co-immunoprecipitation, live-cell imaging, and electrophysiological recordings in transfected mammalian cells and in *Xenopus* oocytes to study heteromerization of Kv2.1 with Kv6.3 and Kv6.4 channels. We describe a mutation in the Zn^{2+} ion-coordinating C3H1 motif of the T1 domain of Kv2.1 that disrupts formation of functional heteromeric channels, but does not prevent formation of homomeric channels.

EXPERIMENTAL PROCEDURES

DNA Constructs—Full-length cDNAs of Kv6.4 (earlier name Kv6.3, GenBank™ accession number AF450108) and Kv6.3 (earlier name Kv10.1 or Kv6.4, GenBank™ accession number AF450110) were obtained by PCR on human brain cDNA (Marathon-Ready cDNA, Clontech, Mountain View, CA). The coding regions of human Kv2.1 (a kind gift of Dr. R. H. Joho, Southwestern University, GenBank™ accession number L02840), Kv6.1 (GenBank™ accession number AF033383), Kv6.3, Kv6.4, and rat Kv1.1 (GenBank™ accession number X12589) were amplified by PCR and cloned into the mammalian expression vectors pcDNA3.1(+) (Invitrogen, Carlsbad, CA) or pIRES (Clontech), or were fused to the E(G/C/Y)FP genes by cloning into the expression vectors pE(G/C/Y)FP-C1 (Clontech). Finally, all constructs were completely sequenced.

Site-directed Mutagenesis—For single amino acid replacement or deletion mutagenesis the QuikChange site-directed mutagenesis kit (Stratagene, La Jolla, CA) was used. Oligonucleotide primers were designed with at least 12 matching nucleotides on each side of an intended nucleotide change. All mutants were completely sequenced.

Direct Interaction Yeast Two-hybrid Assay—The Matchmaker yeast two-hybrid system (Clontech) was used to assay for protein-protein interactions. The T1 domains of rat Kv1.1 (aa 37–142) and human Kv2.1 (aa 31–148), Kv2.2 (accession number AF450111, aa 35–151), Kv6.4 (aa 58–176), and Kv6.3 (aa 11–126) were amplified by PCR and cloned into the yeast DNA-binding domain-containing vector pGBT-9 and the activation domain-containing vector pGAD-424. To check for direct interaction between two proteins 150 ng of both vectors were co-transformed into the yeast strain HF7c according to the manufacturer's protocol. Transformants were plated on medium lacking tryptophan, leucine, and histidine, and incubated for 3–4 days at 30 °C. Yeast transformed with interacting fusion proteins grow as a result of activation of the *HIS3* gene. To determine the strength of the interaction, *HIS3* positive clones were grown on 5–10 mM 3-aminotriazole plates and β-galactosidase assays were performed to verify interaction.

Expression Analysis—Total human and rat tissue RNA was purchased from Clontech and Ambion. Total RNA from the human adrenal gland cell line NCI-H295R (21) or the rat aortic smooth muscle cell line A7r5 was extracted by using HighPure RNA kit (Roche, Mannheim, Germany), which included DNase I digestion. Total RNA (1 μg) eluates were reverse-transcribed (RT) with random hexamers (Applied Biosystems, Foster City, CA) and Superscript II reverse transcriptase (Invitrogen) or Omniscript RT (Qiagen, Hilden, Germany) according to the manufacturers' instructions. Qualitative RT-PCR expression analysis in rat A7r5 cells was performed with AmpliTaq Gold DNA polymerase (Applied Biosystems) using intron-spanning and gene-specific primers for rat Kv channels. The following primers were used: rKv2.1: for 5′-GCTGTGCAGAGAAGAGGAAGA-3′, rev 5′-GTGTTGAGTGACAGAGCGATG-3′; rKv2.2: for 5′-GCCCAGAGAAAAGGAAGAAAC-3′, rev 5′-TGTTGAGAGACAGAGCAATGG-3′; rKv6.3: for 5′-CGTGTCTATGGTGGTGCTGT-3′, rev for 5′-ACCAGCCTATGCAGATAGCTT-3′; rKv6.4: for 5′-CTTGCCTCTCCGTTCTCTTC-3′, rev 5′-ACACAGATGGTCTCCACCAC-3′. Qualitative RT-PCR expression analysis in NCI-H295R cells was performed with human Kv primers, which were also used for quantitative RT-PCR (qPCR). All PCR products showed the expected size and were confirmed by sequencing.

qPCR was performed using an ABI Prism Sequence Detection System 7700 (Applied Biosystems) or an MX3000P real-time PCR system (Stratagene). Specificity of RT-PCR was checked by "no template" and "no RT" controls as well as by melting point analysis. Expression of the target gene was determined as the relative expression (rE) normalized to the housekeeping gene GAPDH ($rE = 1/2^{\Delta Ct}$). The following primers were used for qPCR: rGAPDH: for 5′-GAGAATGGGAAGCTGGTCATCAAC-3′, rev 5′-ACTCCACGACATACTCAGCACCAG-3′; hGAPDH: for 5′-GTCAACGGATTTGGTCGTATT-3′, rev 5′-ACCATGTAGTTGAGGTCAATGAAG-3′; rKv2.1: for 5′-TGCTGTGCAGAGAAGAGGAAGAAA-3′, rev 5′-ACAGGACGATGAACATGATCGAGA-3′; hKv2.1: for 5′-TACTGGAGAAGCCCAATTCCTCTG-3′, rev 5′-CTGTAGCTCAGGCAGCGTGTTG-3′; rKv6.3: for 5′-AGTCTGGATGACCGGAGCAGGTAC-3′, rev 5′-GACGATGAACCGCACGATGCAC-3′; hKv6.3: for 5′-AGCCTGGATGACCGGAGCAGGTAC-3′, rev 5′-CTCACGATGCACTCGGCAGTGAAC-3′; rKv6.4: for 5′-GACTTCAGGGCTGAGGAGGACA-3′, rev 5′-ACAGGCAAAACTCCAGGGAGAAC-3′; hKv6.4: for 5′-TCAGCCTGTGTGTCAGCACCATG-3′, rev 5′-ACGCAGATGGTCTCCACGATGAAA-3′.

Heterologous Expression in HEK293 or COS-7 Cells, Fluorescence Imaging, and Co-immunoprecipitation—HEK293 or COS-7 cells were transfected with 1–2 μg of Kv cDNAs subcloned in the vectors pcDNA3.1 (Invitrogen), pIRES (Clontech) or pE(G/C/Y)FP (Clontech) using Lipofectamine 2000 (Invitrogen) or FuGENE6 (Roche Applied Science).

For immunoprecipitation experiments COS-7 cells were harvested and lysed 24 h after transfection. Immunoprecipitation was performed with anti-Kv2.1 antibodies (Alomone, Israel) and protein A-Sepharose beads (GE Healthcare). After intensive washing the protein-antibody complexes were eluted with SDS-sample buffer, heat-denatured (100 °C) for 5 min, separated on 6 or 8% SDS-polyacrylamide gels and transferred to nitrocellulose membranes. The proteins of interest were visualized by immunostaining the Western blots with anti-Kv2.1 antibodies (Alomone; 1:2000 dilution) or anti-GFP antibodies (Abcam; 1:2500 dilution). The binding of the primary antibodies was detected using peroxidase conjugated goat anti-rabbit antibodies (Pierce; 1:2500 dilu-

tion) and a chemiluminescent extended duration substrate (Super Signal West Dura, Pierce).

Heterologous Expression in CHO-K1 Cells and Electrophysiological Measurements—CHO-K1[2] cells (200,000 cells per 32-mm cell culture dish) were transfected with 1 μg of cDNA coding for Kv subunits in pcDNA3.1 or pIRES and 0.1 μg of pEGFP reporter plasmid using 3.3 μl FuGENE6 (Roche Applied Science).

Patch clamp recordings were carried out on the stage of an inverted microscope (Olympus IX 70) at room temperature (23 °C) 10–24 h after transfection. Adherent CHO-K1 cells in culture dishes, in which an insert was placed to form a low volume chamber, were superfused with the standard extracellular solution (NaCl, 140 mM; KCl, 5.4 mM; $CaCl_2$, 2 mM; $MgCl_2$, 1 mM; glucose, 10 mM; HEPES, 10 mM; titrated to pH 7.4 with NaOH). Data of whole cell recordings were collected with an EPC9 or EPC10 patch clamp amplifier (HEKA, Lambrecht, Germany) using the Pulse software v8.7 (HEKA). For whole cell measurements, patch pipettes made of borosilicate glass (Science Products, Hofheim, Germany) and coated with R-6101 (Dow Chemical, Midland) were used. They had resistances of 2.5 to 4.0 MΩ when filled with the intracellular solution (KCl, 80 mM; potassium-glutamate, 50 mM; Mg-ATP, 2 mM; $MgCl_2$, 2 mM; buffered at 100 nM free Ca^{2+} with 10 mM BAPTA; HEPES, 10 mM; titrated to pH 7.2 with KOH). In whole cell measurements, the liquid junction potentials were +8.0 mV with standard extracellular solution and +4.9 mV with the high K^+ extracellular solution (KCl, 130 mM; $CaCl_2$, 2 mM; $MgCl_2$, 1 mM; glucose, 10 mM; HEPES, 10 mM; titrated to pH 7.4 with KOH), and were corrected by the Pulse software. The osmolarity of all solutions was controlled with a vapor osmometer (Vapro 5520, Wescor Inc., Logan).

The values of pipette and cell membrane capacitance were estimated with the Pulse software and corrected automatically. Series resistance compensation (70–80%) was used to limit voltage errors to less than 5 mV. Only cells with minimal leakage currents were used. The data were acquired at a sampling rate of 5 kHz after filtering at 1.67 kHz. For quantification of the time course of inactivation, the cells were held at a potential of −80 mV and three 30-s depolarizing pulses to 0 mV were applied with an interpulse interval of at least 2 min. The decay of the resulting transient outward currents was fitted with a bi-exponential function. A mono-exponential function was not sufficient to fit the data and tri-exponential functions did not provide a better fit.

The activation characteristics of the Kv channels were determined in symmetrical high-K^+ solution. The cells were depolarized from a holding potential of −80 mV to potentials between −70 and +40 mV (with increments of 10 mV) for 100 ms. Tail current amplitudes arising from subsequent repolarization to −80 mV were measured isochronally immediately after the depolarizing voltage steps. The data were normalized to the tail current obtained after a voltage step to +40 mV and fitted to the modified Boltzmann Equation 1,

$$I_{tail}/I_{max} = 1/(1 + \exp((V_{1/2} - V_m)/k)) \qquad \text{(Eq. 1)}$$

where I_{tail} is the current amplitude at membrane potential V_m, I_{max} is the current amplitude used for normalization, $V_{1/2}$ is the half-activation potential, and k is the slope factor. The values obtained for $V_{1/2}$ and k are reported as means ± S.E.

To confirm the activation curves obtained from tail current measurements in high-K^+ solution we performed additional experiments with standard extracellular solution (5.4 mM K^+). In this case K^+ outward currents were elicited by 1-s depolarizing steps from −80 mV to potentials between −70 and +80 mV applied at intervals of 22 s. The conductance was calculated from the equation: $G = I/(E - E_K)$, where I is the peak current, E is the potential and E_K is the K^+ equilibrium potential (−80.9 mV). The conductance was normalized to the conductance at +80 mV to give G/G_{max}. Activation curves were fitted with the Boltzmann function using a Levenberg-Marquardt algorithm in Origin software v7.5. The results obtained with the two approaches were very similar. The data presented in the results are from the measurements in high-K^+ solution, which had a better signal-to-noise ratio.

Heterologous Expression in Xenopus Oocytes and Voltage Clamp Measurements—The coding regions of Kv2.1, Kv6.3, and Kv6.4 were subcloned in the oocyte expression vector pSGEM. cRNA transcripts were synthesized with a mMessage mMachine T7 kit (Ambion) after vector linearization, purified by precipitation and injected into defolliculated *Xenopus laevis* oocytes at constant amounts, Kv2.1 constructs, 50 pg/oocyte; Kv6.3 constructs, 26 pg/oocyte; Kv6.4 constructs, 30 pg/oocyte. Oocytes were incubated at 19 °C for 46–50 h in ND96 containing (mM): 96 NaCl, 2 KCl, 1 $MgCl_2$, 1 $CaCl_2$, and 5 HEPES (pH 7.4–7.5), supplemented with 0.5 mM theophylline, 100 μg/ml gentamycin, and 2.5 mM sodium pyruvate. Two microelectrode voltage-clamp measurements were performed with a Turbo Tec-10C amplifier (NPI), and data were recorded at a sampling rate of 1 kHz. The oocytes were placed in a small volume perfusion chamber and superfused with ND96 solution. All data were compiled from at least three different batches of oocytes.

FRET Analysis—FRET measurements were carried out with an inverted epifluorescence microscope (IX70, Olympus) using an oil-immersion objective (40×/1.35 NA, Olympus) and a digital video imaging system (TILL-Photonics, Gräfelfing, Germany) equipped with a monochromator. All FRET experiments were performed with live adherent HEK293 cells. FRET efficiencies were determined by monitoring the increase in the ECFP (FRET-donor) fluorescence emission during selective EYFP (FRET-acceptor) photobleaching. The photobleaching protocol for EYFP consisted of 35 cycles of illumination at 512 nm for 4.5 s. The detection protocol for ECFP and EYFP consisted of 45 cycles (10 before bleaching) with 50-ms illumination at 440 nm, followed by a 50-ms delay and 50-ms illumination at 500 nm. The delay between bleaching and detection was 120 ms, and the entire cycle time was 5 s. An intramolecularly fused CFP-YFP tandem protein (kindly provided by Michael Schaefer, Pharmacology, Berlin) resulted in a FRET efficiency of almost 50%. Four or more independent transfections with 3–14 single cells were used for the calculation of FRET efficiency. FRET efficiencies were only accepted when the ratio of fluorescence intensity of EYFP over ECFP was higher than 2.4 and EYFP bleach was greater than 80%.

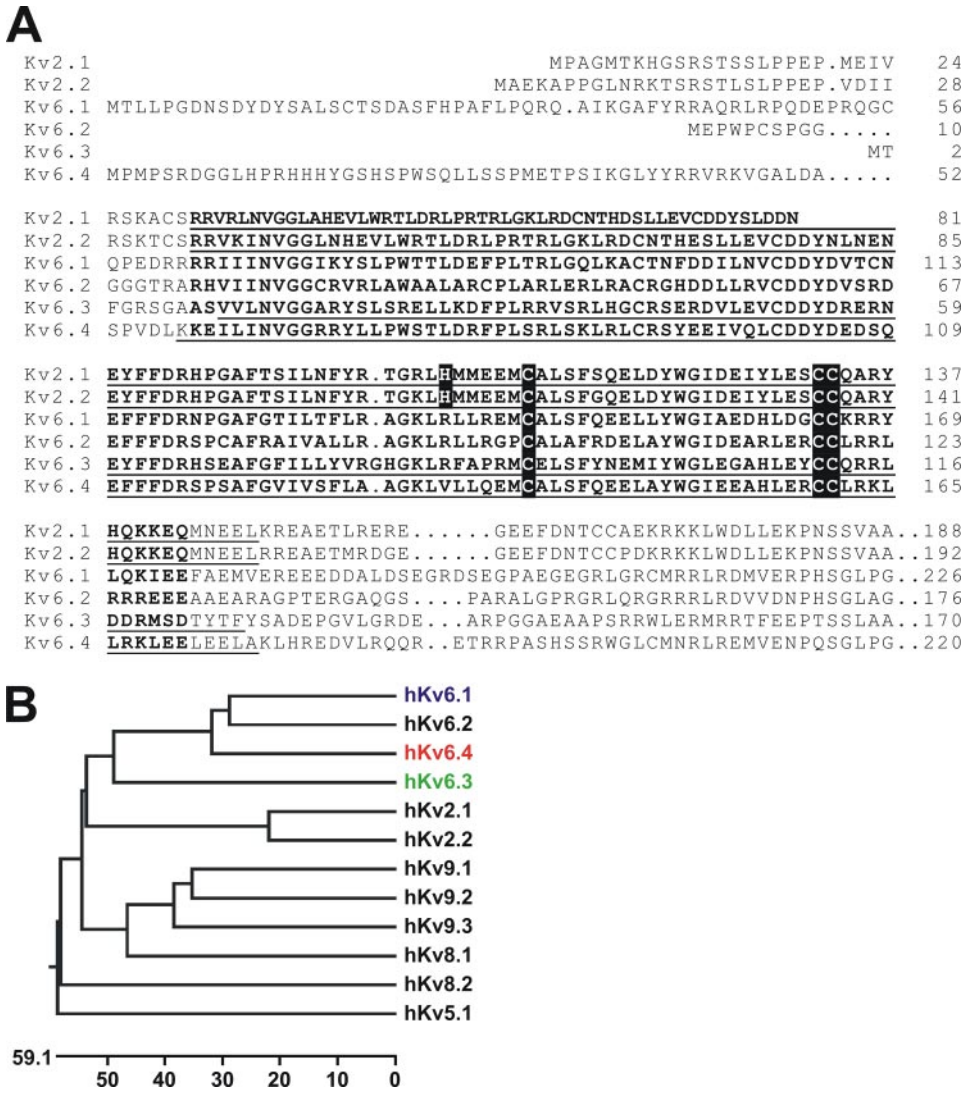

FIGURE 1. **Comparison of human Kv channels.** *A*, alignment of the amino acid sequences of N-terminal regions of Kv2.1, Kv2.2, Kv6.1, Kv6.2, Kv6.3, and Kv6.4. Amino acids are numbered on the *right*. The T1 domain is indicated by *bold letters*. The Zn^{2+} ion coordinating amino acids are highlighted by a *black background*. *Underlined letters* indicate the amino acid regions used for the yeast two-hybrid assay. The alignment was performed with the Clustal algorithm (Heidelberg, UNIX, Sequence Analysis Resources). *B*, phylogenetic tree of the human Kv subfamilies Kv2, Kv5, Kv6, Kv8, and Kv9. The complete coding sequences of Kv channels were analyzed by the MegAlign routine of the DNASTAR Package. The evolutionary distance is shown by the total branch lengths in point-accepted mutation (PAM) units, *i.e.* the mean number of substitutions per 100 residues. The nomenclature used here is according to Gutman *et al.* (43).

RESULTS

Sequence and Predicted Structure of the T1 Domain—To identify a possible T1 domain in the Kv6 channel subunits, the amino acid sequences of human Kv6 were compared with those of the well-characterized Kv2 subfamily (Fig. 1*A*). We found that the cytoplasmic N terminus of all Kv6 subunits contains a conserved non-Shaker T1 domain with an amino acid similarity of 54–66% to the T1 domain of Kv2.1. The T1 domain of Kv6 subunits exhibits one distinctive feature: The histidine (H) of the zinc ion-coordinating C3H1 motif is replaced by arginine (R) (Kv6.1–6.3) or valine (V) (Kv6.4). This substitution of the histidine appears to be characteristic for the Kv6 subfamily. The phylogenetic tree revealed that the Kv2 subfamily is more closely related to the Kv6 subfamily than the to the Kv5, Kv8, and Kv9 subfamilies (Fig. 1*B*). However, unlike the Kv6 subfamily, the Kv5, Kv8, and Kv9 subfamilies harbor a histidine residue in the C3H1 motif, indicating a potential functional relevance of the histidine substitution.

Gene Expression Analysis—Expression profiles of the Kv2.1, Kv6.3, and Kv6.4 channel subunits were examined by quantitative RT-PCR of total RNA isolated from different human and rat tissues (Fig. 2*A*, *upper* and *lower panel*). Robust expression of Kv2.1 could be detected in all tissues examined. Kv2.1 was co-expressed with Kv6.3 and Kv6.4 in human and rat brain and in the adrenal gland. In addition, we found marked co-expression of Kv2.1 with Kv6.3 in human and rat lung, colon, and kidney, and co-expression of Kv2.1 with Kv6.4 in rat heart, lung, liver, colon, and kidney. We also examined the expression Kv2.1 and Kv6.x subunits in eight different brain regions by qPCR (Fig. 2*B*). Again, a strong expression of Kv2.1 as well as co-expression of Kv6.3 and Kv6.4 could be detected in all brain regions examined. Co-expression of Kv2.1 and Kv6.4 subunits was found in the rat aortic smooth muscle cell line A7r5 (Fig. 2*C, upper panel*) and co-expression of Kv2.1 and Kv6.3 was found in the human adrenocortical cell line NCI-H295R (Fig. 2*C, lower panel*).

Co-expression of Kv6 with Kv2.1 Subunits—Kv6.x and/or Kv2.1 subunits were expressed in CHO-K1 cells and the amplitude and kinetics of the resulting currents were analyzed with the whole cell patch-clamp technique. Expression of Kv6.1, Kv6.3, or Kv6.4 subunits alone did not produce any voltage-dependent K^+ current (not illustrated), confirming that these subunits are silent (18, 19, 22). To test for possible formation of heteromeric Kv6.x/Kv2.1 channels we then co-expressed Kv6.1, Kv6.3, or Kv6.4 subunits with Kv2.1 using an IRES-based expression vector in which the transcription of both channel subunits was under the control of the same promoter. This vector induced the translation of two open reading frames from one mRNA transcript. However, the translation of the second open reading frame (Kv2.1) was about 10-fold lower than that of the first one (Kv6), which minimized the formation of homomeric Kv2.1 channels. As illustrated in Fig. 3*A*, the time course of inactivation of the heteromeric channels was much slower than that of homotetrameric Kv2.1 channels. The inactivation could be described by two time constants

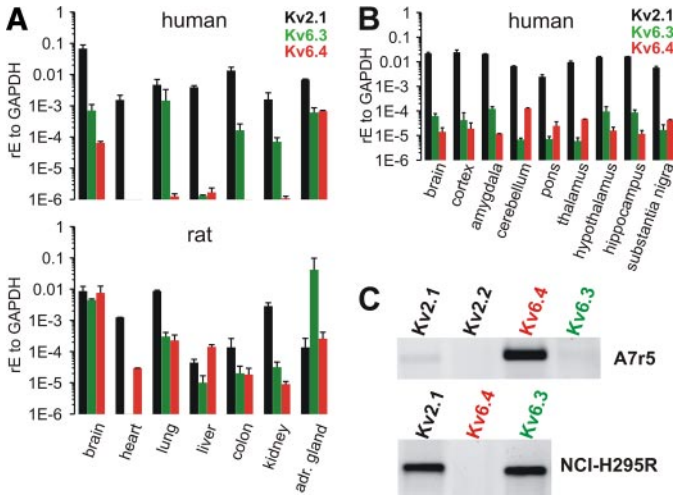

FIGURE 2. **Expression analysis of Kv2.1, Kv6.3, and Kv6.4.** *A*, quantitative gene expression analysis of Kv2.1, Kv6.3, and Kv6.4 mRNAs in different human (*upper panel*) and rat tissues (*lower panel*) by quantitative PCR. *B*, quantitative RT-PCR of Kv2.1, Kv6.3, and Kv6.4 in eight different human brain regions. In *A* and *B*, three independent RT reactions were used. The *bar graphs* show the quantification of the expression (rE) of Kv channels relative to GAPDH. *Error bars* indicate S.E. *C*, representative cell-specific qualitative gene expression analysis of Kv2.1, Kv2.2, Kv6.3, and Kv6.4 in the cell lines A7r5 (*upper panel*) and NCI-H295R (*lower panel*); three independent experiments were performed.

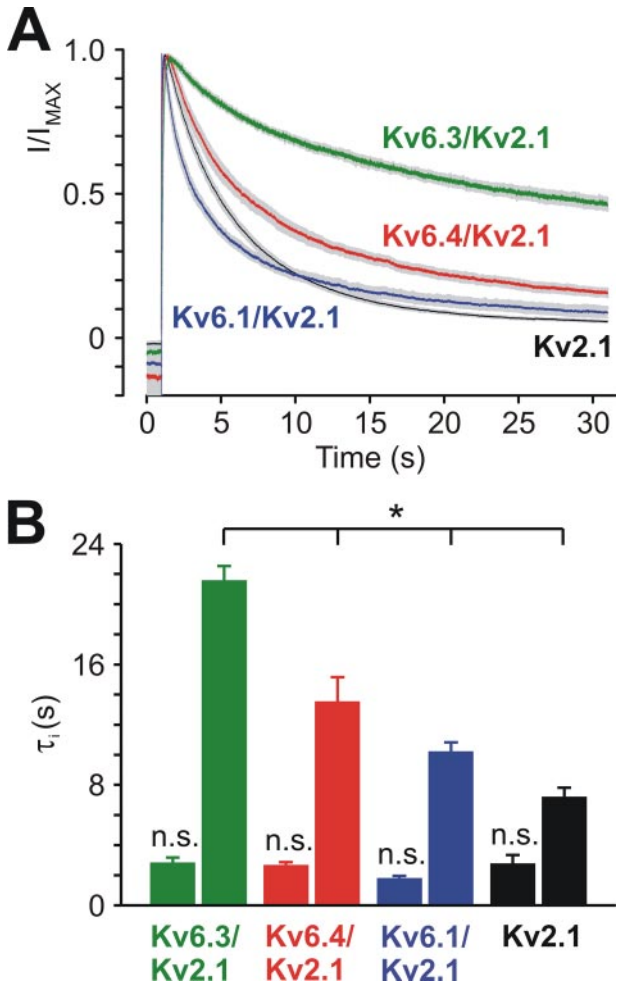

FIGURE 3. **Effects of heteromerization with Kv6 subunits on the time course of inactivation of Kv2. 1 channels.** *A*, Kv6.1 and Kv2.1 ($n = 7$), Kv6.3 and Kv2.1 ($n = 7$), or Kv6.4 and Kv2.1 ($n = 6$) were co-expressed in CHO-K1cells and compared with Kv2.1 subunits expressed alone ($n = 9$; *black line*). Whole cell outward currents were activated by repetitive depolarizing pulses from −80 mV to 0 mV and expressed as fractions of maximal current (I/I_{max}). *Solid lines* represent mean currents; *gray shading* indicates the S.E. *B*, the time course of inactivation was described by two time constants (*left bars*, fast time constant; *right bars*, slow time constants) for each subunit combination; *n.s.*, not significant;*, $p < 0.05$ by one-way analysis of variance with Scheffé post-hoc means comparison.

(see "Experimental Procedures"). The fast time constant was very similar for homomeric Kv2.1 and for heteromeric channels; it had a mean value of about 2.8 s (Fig. 3*B*, see *left bars*). However, the slow time constant of inactivation was significantly different: 7.2 ± 0.6 s for homomeric Kv2.1 channels, 10.2 ± 0.6 s for heteromeric Kv6.1/Kv2.1, 13.5 ± 1.6 s for Kv6.3/Kv2.1 and 21.6 ± 1.0 s for Kv6.4/Kv2.1 channels (Fig. 3*B*, *right bars*).

Residue His-105 of Kv2.1 Is Important for Interaction of the T1 Domains—Because the replacement of the histidine residue in the C3H1 motif is a distinctive property of the Kv6 subfamily, we analyzed whether replacing histidine 105 of Kv2.1 by valine (H105V) would affect the interaction between the T1 domains. Yeast two-hybrid (Y2H) analysis was used to study the interaction between T1 domains of Kv2.1, Kv2.2, Kv6.3, and Kv6.4; the T1 domains analyzed consisted of about 120 amino acids in the N-terminal region of the Kv subunits (*underlined* in Fig. 1*A*). As a negative control, we used the T1 domain of Kv1.1, which does not contain a C3H1 motif. The latter T1 domain interacted exclusively with itself but not with the T1 domains of Kv2 or Kv6 members (Fig. 4*A*), which is consistent with several other studies (10, 11, 23). As expected, T1 domains of wild-type (wt) Kv2.1 and Kv2.2 interacted with themselves and also with the T1 domains of Kv6.3 and Kv6.4 (Fig. 4, *A* and *B*, *left panel*).

An interaction between Kv6.3 and Kv6.4, and interaction of these domains with themselves, could not be detected. However, mutant Kv2.1^{H105V} T1 domains were found to interact with themselves and with wt Kv2.1-T1 domains. Interestingly, co-transformation of mutant Kv2.1^{H105V} with wt Kv6.3 or Kv6.4 T1 domains resulted in loss of interaction (Fig. 4, *A* and *B*, *right panel*). These findings suggest that histidine-105 in Kv2.1 is an important determinant for heteromeric assembly of Kv2.1 with the channel subunits Kv6.3 or Kv6.4 but not for homomeric assembly. Another interesting finding is that replacement of valine 138 in Kv6.4 by histidine resulted in a weak interaction with wt Kv6.4 or mutant Kv6.4^{V138H} T1 domains (Fig. 4*A*) while the analogous mutation in Kv6.3 (Kv6.3^{R84H}) showed no interaction (data not illustrated).

Replacement of Histidine 105 in Kv2.1 Prevents Heterotetrameric Assembly—Because the Y2H direct interaction assays were performed with the detached T1 domains of the Kv channels we tested whether replacement of histidine 105 would also prevent the interaction between the full-length Kv2.1 with Kv6.4 subunits. To address this question we performed co-immunoprecipitation experiments. Kv2.1, Kv2.1^{H105V}, and EGFP-tagged Kv6.4 were heterologously expressed in COS-7 cells and the Kv2.1/Kv6.4 complexes were precipitated from the cell lysates with anti-Kv2.1 antibodies. The immunoprecipitated Kv complexes were analyzed by Western blotting. Probing of the Western blots (Fig. 5*A*) with GFP-specific or Kv2.1-specific antibodies showed that Kv6.4 did co-precipitate with wt Kv2.1

A

BD \ AD	Kv1.1	Kv2.1	Kv2.2	Kv6.4	Kv6.3	Kv2.1^{H105V}	Kv6.4^{V138H}
Kv1.1	+++	-	-	-	-	-	-
Kv2.1	-	+++	+++	+++	+++	+	+++
Kv2.2	-	+++	+++	+++	+++	++	+++
Kv6.4	-	+++	++	-	-	-	+
Kv6.3	-	+++	+++	-	-	-	-
Kv2.1^{H105V}	-	+++	+++	-	-	+	-
Kv6.4^{V138H}	-	+++	+++	+	-	-	+

B

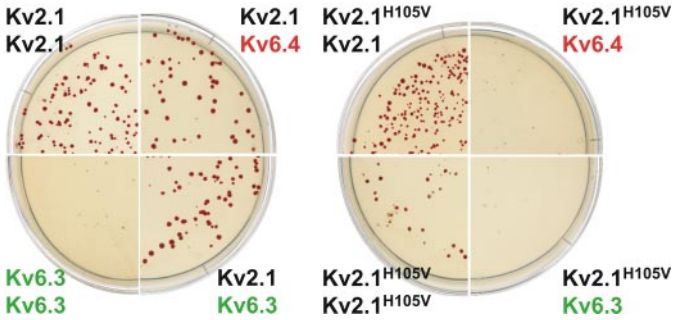

FIGURE 4. **T1 domain interaction as assessed by yeast two-hybrid analysis.** *A*, interaction of the T1 domains of Kv2.1, Kv2.2, Kv6.3, and Kv6.4. The T1 domain of Kv1.1 was used as a negative control. The strength of the interaction is indicated by the number of + signs. +++ indicates interaction as strong as the interaction between Kv2.1 fused to the activation domain (*AD*) with Kv2.1 fused to the binding domain (*BD*); − denotes no growth of transformants and a negative β-galactosidase test. Each interaction assay was repeated three times. *B*, typical examples of yeast two-hybrid analysis of the interaction between different T1 domains (*left panel*, wt; *right panel*, mutant H105V T1 domain of Kv2.1). To check for interaction, transformants were plated on medium lacking tryptophan, leucine, and histidine.

A

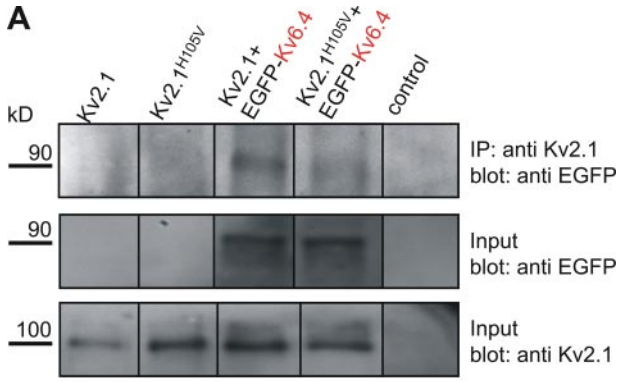

B

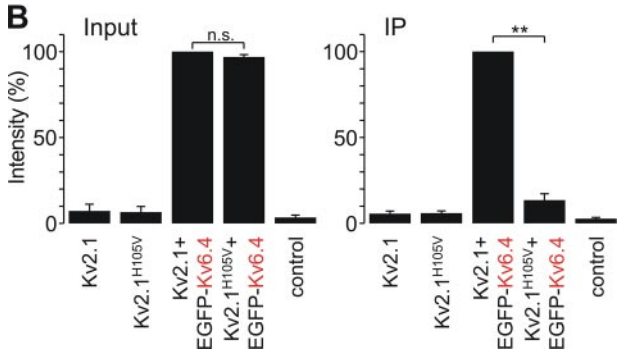

FIGURE 5. **Co-immunoprecipitation of EGFP-tagged Kv6.4 with Kv2.1.** *A*, cell lysates of COS-7 cells transfected with Kv2.1, Kv2.1^{H105V}, Kv2.1 + EGFP-Kv6.4, or Kv2.1^{H105V} + EGFP-Kv6.4 or of non-transfected cells (control) were immunoprecipitated (*IP*) with anti-Kv2.1 antibodies. The Western blots of the precipitated protein complexes were immunodecorated with anti-GFP antibodies (*upper panel*). To check for equal heterologous expression of EGFP-Kv6.4 and Kv2.1 COS-7 cell lysates (*Input*) were probed on Western blots by immunostaining with anti-GFP and anti-Kv2.1 antibodies, respectively (*middle* and *lower panel*). *B*, the intensities of the protein bands of interest (EGFP-Kv6.4) from three independent experiments were quantified (in arbitrary units) and corrected for background using the TINA densitometry software. The relative expression in % in comparison with Kv2.1 + EGFP-Kv6.4 is plotted. *n.s.*, not significant; **, $p < 0.01$ by unpaired Student's *t* test.

but not with the mutant Kv2.1^{H105V} (Fig. 5*A* (*upper panel*) and *B* (*right panel*)). The input controls (Fig. 5*A*, *middle* and *lower panels*; 5*B*, *left panel*) show that equal amounts of EGFP-tagged Kv6.4, Kv2.1, and Kv2.1^{H105V} subunits were expressed. This result indicates that the histidine 105 in Kv2.1 is crucial for the heterotetramerization of full-length Kv2.1 and Kv6.4 subunits.

To examine channel assembly in intact cells we used a FRET approach. Full-length Kv subunits, whose N termini were tagged with EYFP and ECFP, were transiently expressed in HEK293 cells and studied by live cell imaging. FRET efficiencies were determined by measuring the increase in ECFP fluorescence emission during selective EYFP photobleaching (ECFP was the FRET-donor and EYFP the FRET-acceptor). Detection of a significant level of FRET between the two different fluorescent molecules was used as an indicator of channel assembly. As a positive control we analyzed homomeric assembly of Kv2 channels. ECFP-Kv2.1 co-expressed with EYFP-Kv2.1 showed a typical time course of increase in ECFP intensity over initial levels (Fig. 6*A*), and the same result was obtained with ECFP-Kv1.1 and EYFP-Kv1.1 (Fig. 6*A*).

In contrast, the combination of Kv1.1 and Kv2.1 produced no measurable FRET signal during EYFP photobleaching. On average, a FRET efficiency of more than 20% was obtained for homomeric combinations and a FRET signal of 1.5 ± 0.3% for the non-interacting channel combination (Fig. 6*B*). Consistent with our Y2H analysis, co-expression of Kv2.1 with Kv6.3 or 6.4 subunits generated FRET signals of more than 20%. However, when Kv6.3 or Kv6.4 were co-expressed with the mutants Kv2.1^{H105V} or Kv2.1^{H105R} a highly significant reduction in FRET efficiency was found (Fig. 6*C*). The combination of the non-interacting subunits Kv6.3 or Kv6.4 with themselves or with Kv1.1 also displayed low FRET efficiencies. When the FRET donor and the FRET acceptor in the different subunits were exchanged, the same results were obtained; for example, the inverse combination ECFP-Kv2.1/EYFP-Kv6.3 was associated with a FRET efficiency of 24.8 ± 1.4% ($n = 24$ from 4 transfections; not illustrated), which is very similar to the example shown in Fig. 6*C* (*first green bar*).

Interestingly, FRET signals for homomeric assembly of Kv2.1^{H105V} or Kv2.1^{H105R} subunits were significantly higher than for their wt counterparts (Fig. 6*D*). Nevertheless, the current amplitude measured with the mutant channels in the cell membrane was almost the same as of wt channels (supplemental Fig. S1), which suggests that higher FRET efficiencies do not necessarily result in a better surface expression. However, the homomeric mutant channels differed substantially from wt Kv2.1 in their activation and inactivation kinetics (Fig. 8, *B*–*D*). An additional slow time constant of activation was observed in Kv2.1^{H105R} and Kv2.1^{H105V} and the slow time constants of inactivation were about 6-fold longer (Fig. 8*C*).

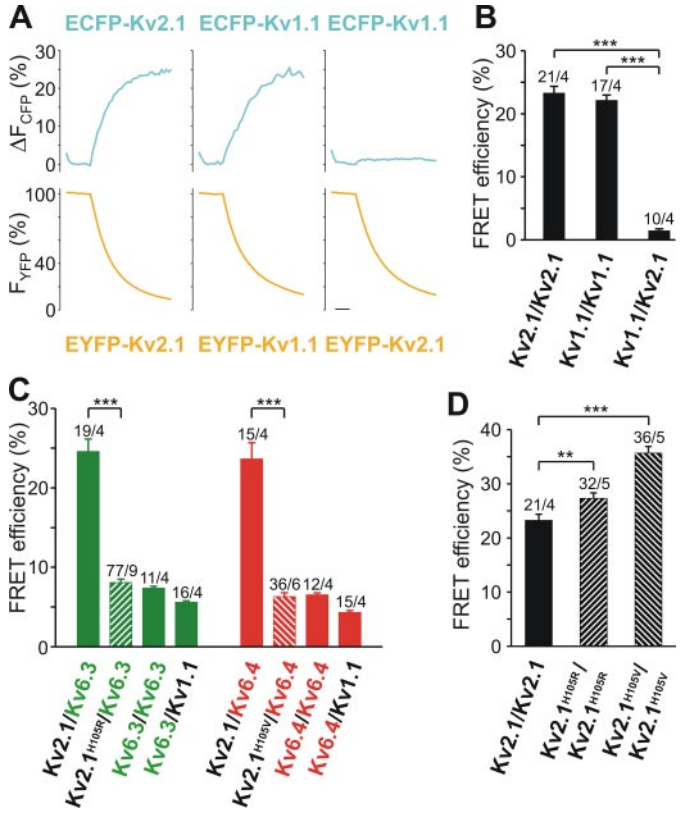

FIGURE 6. **FRET analysis of protein interaction.** Heterologously expressed Kv subunits whose N termini were tagged with EYFP or ECFP were analyzed by EYFP photobleaching in live HEK293 cells. *A*, three examples of the typical time course of normalized fluorescence intensities from one cell without the region of nucleus are displayed. *Scale bar*, 30 s. *B–D*, normalized FRET efficiencies for different combinations of Kv subunits; in *C*, the subunits indicated first were EYFP-tagged. *Bars* represent means ± S.E. *Numbers* above the bars indicate the total number of cells from which the data were derived and the number of independent transfections. ***, $p < 0.001$ by unpaired Student's *t* test.

To further characterize the possible roles of the crucial residues in the T1 domain (position 84 in Kv6.3 and position 138 in Kv6.4) in preventing homomeric channel assembly of Kv6.x channels we performed additional FRET measurements. In either Kv6 subunit we replaced these residues by histidine, which is at the corresponding position in Kv2.1. Supplemental Fig. S2*A* shows that Kv6.3^{R84H} and Kv6.4^{V138H} displayed FRET efficiencies of less than 5%, indicating the absence of channel assembly (supplemental Fig. S2*A*). These findings confirm the results of our Y2H analysis. Consistent with these data, live-cell imaging experiments showed that neither wt nor mutant Kv6.3 or Kv6.4 channels were localized to the surface membrane (supplemental Fig. S2*B*). In conclusion, introducing a histidine residue, which is part of the Zn^{2+}-coordinating C3H1 motif in Kv2.1, at the corresponding position in Kv6.3 and Kv6.4 did not lead to the formation of homomeric Kv6 channels.

Replacement of Histidine 105 Prevents Formation of Functional Heterotetrameric Channels—Homomeric Kv2.1 und heteromeric Kv2.1/Kv6 channels differ not only in their rate of inactivation (Fig. 3) but also in some other functional characteristics. One example is the rate of deactivation, determined by the analysis of tail currents (Fig. 7*A*). The rate of deactivation was much slower in the heteromeric channels. Another distinc-

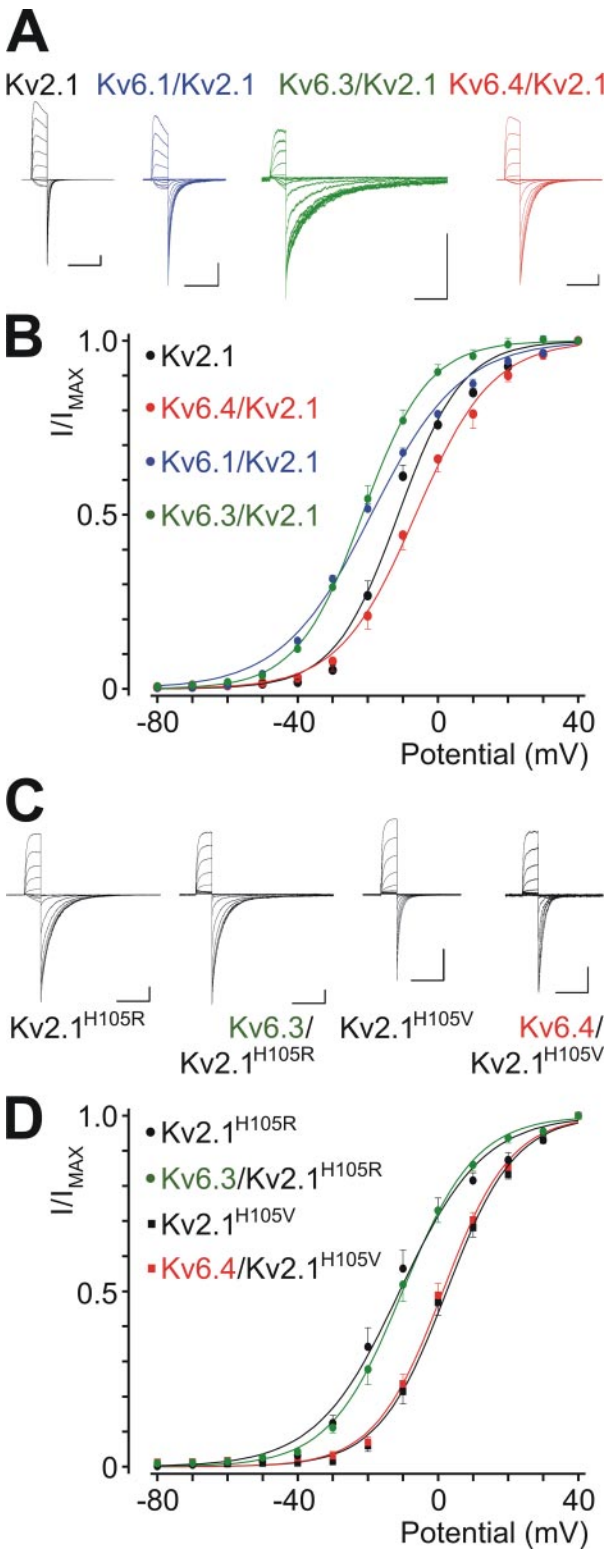

FIGURE 7. **Functional analysis of heteromerization using whole cell measurements in CHO-K1 cells.** The cells were superfused with symmetrical high K^+ solutions and depolarizing voltage steps were applied from the holding potential of −80 mV to potentials between −70 and +40 mV (10 mV increments). *A*, typical currents elicited after transfection of the subunits indicated; *scale bars*, 200 ms, 1 nA. *B*, voltage dependence of activation obtained from the amplitudes of the tail currents; means ± S.E. of 4–6 cells are presented. *C*, typical currents elicited after transfection of the Kv2.1 mutants and the Kv6.x subunits indicated; *scale bars*, 200 ms, 1, 1, 5, and 0.2 nA (*from left to right*). *D*, voltage dependence of activation obtained from the amplitudes of tail currents; means ± S.E. of 6–8 cells are presented.

tive feature is the activation curve of the channels, which was calculated from the amplitudes of the tail currents (see "Experimental Procedures"). Homomeric Kv2.1 channels were half-maximally activated at -11.3 ± 0.9 mV with a slope factor k of 9.2 ± 0.8 mV as derived from the Boltzmann fit (Fig. 7*B*). Co-expression of Kv2.1 with Kv6.1 or Kv6.3 channel subunits resulted in a marked leftward shift of the activation curve. In the case of co-expression of Kv2.1 with Kv6.1, an increase in the slope factor k to 12.8 ± 0.6 mV was also noted (Fig. 7*B*). A characteristic rightward shift of almost 5 mV was observed after the co-expression of Kv2.1 with Kv6.4, with half-maximal activation at -6.4 ± 0.4 mV.

Changes in these functional characteristics were used as a test for the role of the histidine residue at position 105 of Kv2.1 in heteromeric assembly of the different subunits. Expression of Kv2.1^{H105V} or Kv2.1^{H105R} subunits alone resulted in voltage-dependent currents with a slower deactivation than the wt counterparts (compare Fig. 7, *C* and *A*, *left*). In addition, homomeric Kv2.1^{H105V}, but not homomeric Kv2.1^{H105R} channels, showed a significant rightward shift of the activation curve by about 14 mV compared with wt channels (Fig. 7, *B* and *D*). Co-expression of Kv2.1^{H105R} with Kv6.3 or co-expression of Kv2.1^{H105V} with Kv6.4 affected neither the rate of deactivation (Fig. 7*C*) nor the position of the activation curve (Fig. 7*D*), which suggests that heteromeric assembly was impaired or abolished by the replacement of His-105 by valine or arginine.

We then performed an additional series of experiments in which Kv2.1 and Kv6.x subunits were co-expressed in *Xenopus* oocytes (Fig. 8). This expression system has the advantage that precisely controlled amounts of cRNA can be co-injected. In *Xenopus* oocytes, too, co-expression of Kv2.1 with Kv6.3 or Kv6.4 led to marked reduction in the rates of activation and inactivation (Fig. 8*A*), and both Kv2.1H^{105R} and Kv2.1H^{105V} showed marked changes in their rates of activation and inactivation (Fig. 8, *B* and *C*) compared with wt Kv2.1. Co-expression of the mutants Kv2.1^{H105R} (Fig. 8*D*) or Kv2.1^{H105V} (not illustrated) with Kv6.3 or Kv6.4 had no further effects on channel kinetics.

The leftward shift of the activation curve after co-expression of Kv2.1 with Kv6.3 and the prominent rightward shift of the activation curve of Kv2.1^{H105V} were confirmed in the oocyte expression system (Fig. 8*E*). The mutant Kv2.1^{H105R} displayed a slight rightward shift of the activation curve (Fig. 8*E*). Co-expression of Kv2.1^{H105R} with Kv6.3 and co-expression of Kv2.1^{H105V} with Kv6.4 produced no further shift in the position of the activation curve.

Finally, we tested the role of histidine 105 in Kv2.1/Kv6.3 heteromerization by constructing dominant-negative mutants of Kv2.1^{H105R} and of Kv6.3. Loss of K^+ permeability was induced by exchanging the two glycine residues in the K^+ channel signature motif by alanines (changing the GYG motif to AYA). Expression of AYA-Kv2.1^{H105R} subunits in *Xenopus* oocytes produced no measurable current (Fig. 8*F*), indicating that channels with the AYA mutation are non-conducting. Co-expression of Kv2.1^{H105R} subunits with AYA-Kv2.1^{H105R} subunits produced a strong dominant-negative effect, *i.e.* the currents measured after co-injection of both cRNAs were reduced to 8% of control. These findings suggest that assembly of the subunits was not disturbed by the AYA mutation and that the presence of one AYA subunit was sufficient to render the channel non-functional. In contrast, co-expression of Kv2.1^{H105R} with AYA-Kv6.3 had no significant effect of current amplitude, confirming that the mutation of histidine 105 of Kv2.1 prevented heteromeric assembly of Kv2.1 with Kv6.3 subunits, but not homotetrameric assembly.

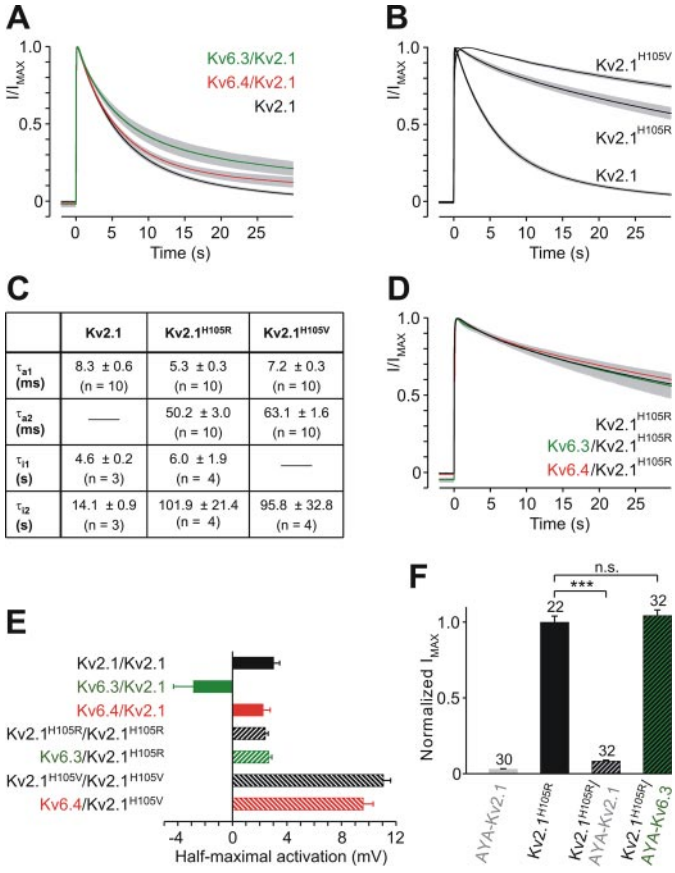

FIGURE 8. **Biophysical properties of Kv2.1 mutants and Kv2.1/Kv6 heteromeric channels expressed in *Xenopus* oocytes.** Outward currents were elicited by depolarizing pulses from -80 mV to $+40$ mV to potentials between -20 and $+40$ mV (with increments of 10 mV) for 30 s. *A*, effects of co-injection of Kv6.3 or Kv6.4 on the time course of inactivation of Kv2.1. In *A*, *B*, and *D* currents are expressed as fractions of maximal current (I/I_{max}); *solid lines* represent mean currents of 3–4 oocytes, *gray shading* indicates the S.E. *B*, effects of mutations of residue His-105 on the time course of inactivation of Kv2.1. *C*, time constants of activation and inactivation ($\pm$ S.E.) of Kv2.1 and the mutants Kv2.1^{H105R} and Kv2.1^{H105V}. Activation (τ_a) and inactivation (τ_i) were fitted with two exponentials, except for τ_a of wt Kv2.1 and τ_i of Kv2.1^{H105V}, where the time course was adequately described by a single exponential. *D*, effects of co-injection of Kv6.3 or Kv6.4 on the time course of inactivation of Kv2.1^{H105R}. *E*, potential of half-maximal activation of Kv2.1, Kv2.1 mutants, and heteromeric Kv2.1/Kv6 channels. The conductance was calculated from the equation: $G = I/(E - E_K)$, where I is the peak current, E is the potential, and E_K is the K^+ equilibrium potential (-90.0 mV). The conductance was normalized to the conductance at $+40$ mV to give G/G_{max}. cRNA coding for the subunits indicated was injected at equimolar amounts. For each combination, four activation curves were fitted with the Boltzmann function and the resulted half-maximal activation potentials are presented as means $\pm$ S.E. *F*, normalized peak current amplitude (at $+40$ mV) measured 46–50 h after injection of cRNA coding for the indicated subunits. For the subunit combinations Kv2.1^{H105R}:AYA-Kv2.1 and Kv2.1^{H105R}:AYA-Kv6.3 the molar ratio of the co-injected cRNA was 1:2. The number of oocytes from which the data were obtained is given *above* the bars; three different batches of oocytes were used. *n.s.*, not significant; ***, $p < 0.001$ by unpaired Student's *t* test.

DISCUSSION

We have studied the functional significance of the C3H1 motif for homomeric and heteromeric assembly of Kv2 and Kv6 subunits. We found that replacement of the histidine residue in the Zn^{2+} ion-coordinating C3H1 motif of the T1 domain of Kv2.1 by arginine ($Kv2.1^{H105R}$) or by valine ($Kv2.1^{H105V}$) had the following effects: (i) In the yeast-two-hybrid assay, the T1 domain of $Kv2.1^{H105V}$ failed to interact with the T1 domains of Kv6.3 and Kv6.4, (Fig. 4*A*). (ii) Kv6.4 was co-immunoprecipitated with wt Kv2.1 but not with $Kv2.1^{H105V}$ (Fig. 5*B*). (iii) After co-expression of the mutants $Kv2.1^{H105R}$ or $Kv2.1^{H105V}$ with Kv6.3 or Kv6.4 FRET efficiencies were strongly reduced compared with wt Kv2.1 (Fig. 6*C*). (iv) Co-expression of wt Kv2.1 with Kv6.3 or Kv6.4 in a mammalian cell line had pronounced effects on the time course of activation, deactivation and inactivation and on the voltage-dependence of activation of Kv2.1, whereas co-expression of the mutants $Kv2.1^{H105R}$ or $Kv2.1^{H105V}$ with Kv6.3 or Kv6.4 did not modify the biophysical properties of the mutant channels at all (Fig. 7*D*). (v) These findings were confirmed by co-expression of the same mutants in *Xenopus* oocytes (Fig. 8). (vi) Co-expression experiments with dominant-negative mutants in *Xenopus* oocytes showed that the mutant $Kv2.1^{H105R}$ subunits cannot co-assemble with Kv6.3 (Fig. 8*F*). Taken together, these findings suggest that mutation of the histidine residue in the Zn^{2+} ion-coordinating C3H1 motif of the T1 domain of Kv2.1 disrupts the formation of functional heteromeric Kv2.1/Kv6 channels.

Homomeric assembly of Kv2.1 channels was not affected at all by mutation of the histidine residue at position 105 ($Kv2.1^{H105R}$ and $Kv2.1^{H105V}$). In addition to interaction of Kv2.1 T1 domains with themselves (Fig. 4*A*) we observed functional homomeric assembly of $Kv2.1^{H105R}$ and $Kv2.1^{H105V}$ channels (Figs. 6*D*, 7*C*, and 8*E*). These findings show that alteration of the C3H1 motif alone is not sufficient to suppress homotetramerization of Kv2.1. In this respect Kv2.1 channels markedly differ from Kv4.2 channels, where mutation of the homologous histidine residue (His-104) abolished functional expression (14).

In the reverse experiment, introducing a histidine residue, which is part of the Zn^{2+}-coordinating C3H1 motif in Kv2.1, at the corresponding position in Kv6.3 and Kv6.4 did not facilitate homomeric interaction of Kv6.x channels (supplemental Fig. S2*A*). Thus the difference in the C3H1 motif cannot fully explain the lack of homomeric assembly of Kv6.3 and Kv6.4 channels. There must be additional structural determinants that promote or prevent tetramerization, for example other polar interactions in the T1 domain (12) or subunit interaction motifs in the transmembrane domains of Kv channels (7, 14) or in the C termini (24, 25).

Several previous studies have addressed the role of the T1 domain in the intracellular N terminus of Kv channels. The T1 domain has been shown to be involved in various processes such as subunit-specific assembly (8, 9, 16, 18, 19, 26–30) in early biogenesis of the channels (6), in binding of cytosolic auxiliary subunits (31, 32) and in the gating of channels inserted in the cell membrane (33–36). In addition, it has been shown that the assembly of Kv subunits possessing C3H1 motifs is impaired when zinc is depleted (13, 14). The results presented here were obtained in the presence of physiological zinc ion concentrations, indicating that all effects described here are not the result of zinc depletion.

Our data demonstrate that heteromerization changes the biophysical properties of the channels, for example, inactivation and deactivation kinetics and the voltage dependence of activation. The influence of heteromerization on deactivation kinetics has been discussed controversially in the literature (18, 19). In agreement with Sano *et al.* (18), our data show a marked slowing of deactivation kinetics in Kv2.1/Kv6.3 heteromers. No change in the rate of deactivation of these heteromers was found by Ottschytsch *et al.* (19) (in their nomenclature Kv2.1/Kv10.1). In contrast to both of these groups (18, 19), we found that heteromerization gave rise to a distinct shift in the half-maximal activation potential ($V_{1/2}$): with homomeric Kv2.1 channels $V_{1/2}$ was about −11 mV, with heteromeric Kv2.1/Kv6.3 channels $V_{1/2}$ was −22 mV; with heteromeric Kv2.1/Kv6.4 channels $V_{1/2}$ was around −6 mV, *i.e.* the shift was in the opposite direction. We determined these shifts in the voltage dependence of activation using two different approaches, (i) patch-clamp recordings in co-transfected in CHO-K1 cells (Fig. 3) and (ii) two-electrode voltage clamp in *Xenopus* oocytes co-injected with different cRNAs (Fig. 8); the two series of experiments gave very similar results. The discrepancy between our data and those of the two previous reports may be related to the fact that we used CHO-K1 cells and an IRES-based expression vector (where formation of homomeric channels was minimized) whereas the other groups used a fibroblast cell line stably overexpressing Kv2.1 (18) or simple co-transfection of two plasmids in murine fibroblast cells (19).

In conclusion, our results suggest that Kv2.1 subunits are capable of forming both homomeric Kv2.1 channels and heteromeric Kv2.1/Kv6.x channels, whereas Kv6.x subunits cannot assemble as homomeric channels. Mutation of the critical histidine residue in the T1 domain of Kv2.1 prevented formation of Kv2.1/Kv6.x heteromeric channels but not homomeric assembly of Kv2.1. Thus, the restriction in combinatorial possibilities may be partially attributable to the complementary properties of the T1 domains of Kv2.1 and Kv6.x. However, since the introduction of the histidine at the corresponding position of Kv6.3 or Kv6.4 was not sufficient to permit homomeric assembly of these subunits, other subunit interaction domains may also play a role in determining subunit composition of Kv channels.

The results of our quantitative gene expression analysis suggest that Kv2.1 subunits are ubiquitously expressed, in agreement with previous studies (37), whereas the expression pattern of Kv6 subunits is more restricted. Because co-expression of Kv2 and Kv6 subunits could be detected in several different tissues it is tempting to speculate that heterotetramerization of Kv2.1 and Kv6.x channels may be functionally relevant by allowing fine-tuning of the biophysical properties of Kv channels according to the actual cellular demand. This may be particularly important in central neurons, where Kv2.1 channels have been shown to cluster in the somatic and in the proximal dendritic membranes and to constitute the majority of the delayed rectifier current. This current plays a major role in the

regulation of synaptic excitation in dendrites, especially during high frequency firing (38–40) and during ischemia (41). In addition to modulating channel kinetics, heteromerization with Kv6.3 or Kv6.4 might also influence the trafficking of Kv2.1 from the endoplasmic reticulum to the surface membrane channels, their turnover rate at the surface membrane, and their interaction with accessory proteins (37, 42).

Acknowledgments—We thank Eva Braun, Tanja Haase, and Daniela Wagner for expert assistance with cell culture and Andrea Schubert for excellent molecular biological assistance. We also thank Tim Plant for critical advice on the manuscript. The support by Robert Graf and Ekkehard Schüler in the mechanical workshop is greatly appreciated. We are grateful to Vladimir Chubanov for his initial help with the FRET technique.

REFERENCES

1. Hille, B. (2001) *Ion Channels of Excitable Membranes*, 3rd Ed., pp. 131–167. Sinauer Associates, Inc., Sunderland
2. Rudy, B. (1988) *Neuroscience* **25,** 729–749
3. Jan, L. Y., and Jan, Y. N. (1997) *J. Physiol.* **505,** 267–282
4. Coetzee, W. A., Amarillo, Y., Chiu, J., Chow, A., Lau, D., McCormack, T., Moreno, H., Nadal, M. S., Ozaita, A., Pountney, D., Saganich, M., Vega-Saenz de Miera, E., and Rudy, B. (1999) *Ann. N. Y. Acad. Sci.* **868,** 233–285
5. Barry, D. M., and Nerbonne, J. M. (1996) *Annu. Rev. Physiol.* **58,** 363–394
6. Lu, J., Robinson, J. M., Edwards, D., and Deutsch, C. (2001) *Biochemistry* **40,** 10934–10946
7. Deutsch, C. (2002) *Annu. Rev. Physiol.* **64,** 19–46
8. Robinson, J. M., and Deutsch, C. (2005) *Neuron* **45,** 223–232
9. Xu, J., Yu, W., Jan, Y. N., Jan, L. Y., and Li, M. (1995) *J. Biol. Chem.* **270,** 24761–24768
10. Li, M., Jan, Y. N., and Jan, L. Y. (1992) *Science* **257,** 1225–1230
11. Shen, N. V., Chen, X., Boyer, M. M., and Pfaffinger, P. J. (1993) *Neuron* **11,** 67–76
12. Bixby, K. A., Nanao, M. H., Shen, N. V., Kreusch, A., Bellamy, H., Pfaffinger, P. J., and Choe, S. (1999) *Nat. Struct. Biol.* **6,** 38–43
13. Jahng, A. W., Strang, C., Kaiser, D., Pollard, T., Pfaffinger, P., and Choe, S. (2002) *J. Biol. Chem.* **277,** 47885–47890
14. Strang, C., Kunjilwar, K., DeRubeis, D., Peterson, D., and Pfaffinger, P. J. (2003) *J. Biol. Chem.* **278,** 31361–31371
15. Tu, L., Santarelli, V., Sheng, Z., Skach, W., Pain, D., and Deutsch, C. (1996) *J. Biol. Chem.* **271,** 18904–18911
16. Zhu, X. R., Netzer, R., Bohlke, K., Liu, Q., and Pongs, O. (1999) *Receptors Channels* **6,** 337–350
17. Vega-Saenz de Miera, E. C. (2004) *Brain Res. Mol. Brain Res.* **123,** 91–103
18. Sano, Y., Mochizuki, S., Miyake, A., Kitada, C., Inamura, K., Yokoi, H., Nozawa, K., Matsushime, H., and Furuichi, K. (2002) *FEBS Lett.* **512,** 230–234
19. Ottschytsch, N., Raes, A., Van Hoorick, D., and Snyders, D. J. (2002) *Proc. Natl. Acad. Sci. U. S. A.* **99,** 7986–7991
20. Kramer, J. W., Post, M. A., Brown, A. M., and Kirsch, G. E. (1998) *Am. J. Physiol.* **274,** C1501–C1510
21. Rainey, W. E., Bird, I. M., and Mason, J. I. (1994) *Mol. Cell. Endocrinol.* **100,** 45–50
22. Post, M. A., Kirsch, G. E., and Brown, A. M. (1996) *FEBS Lett.* **399,** 177–182
23. Covarrubias, M., Wei, A. A., and Salkoff, L. (1991) *Neuron* **7,** 763–773
24. Ju, M., Stevens, L., Leadbitter, E., and Wray, D. (2003) *J. Biol. Chem.* **278,** 12769–12778
25. Mohapatra, D. P., Siino, D. F., and Trimmer, J. S. (2008) *J. Neurosci.* **28,** 4982–4994
26. Chiara, M. D., Monje, F., Castellano, A., and Lopez-Barneo, J. (1999) *J. Neurosci.* **19,** 6865–6873
27. Hugnot, J. P., Salinas, M., Lesage, F., Guillemare, E., de Weille, J., Heurteaux, C., Mattei, M. G., and Lazdunski, M. (1996) *EMBO J.* **15,** 3322–3331
28. Salinas, M., de Weille, J., Guillemare, E., Lazdunski, M., and Hugnot, J. P. (1997) *J. Biol. Chem.* **272,** 8774–8780
29. Salinas, M., Duprat, F., Heurteaux, C., Hugnot, J. P., and Lazdunski, M. (1997) *J. Biol. Chem.* **272,** 24371–24379
30. Patel, A. J., Lazdunski, M., and Honore, E. (1997) *EMBO J.* **16,** 6615–6625
31. Long, S. B., Campbell, E. B., and MacKinnon, R. (2005) *Science* **309,** 897–903
32. Pioletti, M., Findeisen, F., Hura, G. L., and Minor, D. L., Jr. (2006) *Nat. Struct. Mol. Biol.* **13,** 987–995
33. Wang, G., Shahidullah, M., Rocha, C. A., Strang, C., Pfaffinger, P. J., and Covarrubias, M. (2005) *J. Gen. Physiol.* **126,** 55–69
34. Wang, G., and Covarrubias, M. (2006) *J. Gen. Physiol.* **127,** 391–400
35. Cushman, S. J., Nanao, M. H., Jahng, A. W., DeRubeis, D., Choe, S., and Pfaffinger, P. J. (2000) *Nat. Struct. Biol.* **7,** 403–407
36. Minor, D. L., Lin, Y. F., Mobley, B. C., Avelar, A., Jan, Y. N., Jan, L. Y., and Berger, J. M. (2000) *Cell* **102,** 657–670
37. Vacher, H., Mohapatra, D. P., and Trimmer, J. S. (2008) *Physiol. Rev.* **88,** 1407–1447
38. Du, J., Haak, L. L., Phillips-Tansey, E., Russell, J. T., and McBain, C. J. (2000) *J. Physiol.* **522,** 19–31
39. Malin, S. A., and Nerbonne, J. M. (2002) *J. Neurosci.* **22,** 10094–10105
40. Misonou, H., Mohapatra, D. P., and Trimmer, J. S. (2005) *Neurotoxicology* **26,** 743–752
41. Misonou, H., Thompson, S. M., and Cai, X. (2008) *J. Neurosci.* **28,** 8529–8538
42. Misonou, H., and Trimmer, J. S. (2005) *J. Neurosci. Methods* **144,** 165–173
43. Gutman, G. A., Chandy, K. G., Grissmer, S., Lazdunski, M., McKinnon, D., Pardo, L. A., Robertson, G. A., Rudy, B., Sanguinetti, M. C., Stuhmer, W., and Wang, X. (2005) *Pharmacol. Rev.* **57,** 473–508